CYBERNETICS AND PHYSICS, VOL. 11, NO. 1, 2022, 30–36

A SPACE ROBOT CONTROL AT APPROACHING AND INSPECTING A GEOSTATIONARY SATELLITE STATE

Yevgeny Somov
Navigation, Guidance and Control
Samara State Technical University
Russia
e_somov@mail.ru

Sergey Butyrin
Navigation, Guidance and Control
Samara State Technical University
Russia
butyrinsa@mail.ru

Tatyana Somova
Navigation, Guidance and Control
Samara State Technical University
Russia
te_somova@mail.ru

Article history:
Received 02.05.2022, Accepted 25.05.2022

Abstract

The problems of approaching a space robot to a geostationary satellite and visual checking its technical state are considered. The robot's control system uses both plasma and catalytic electric propulsion units as well as a cluster of four control moment gyros. The simulation results of the developed guidance and control algorithms are presented that demonstrate their effectiveness.

Key words

Space robot, guidance, control, geostationary satellite, approaching, visual inspection.

Abbreviations

AM = Angular Momentum
AOCS = Attitude and Orbit Control System
BRF = Body Reference Frame
CPU = Chemical Propulsion Unit
EPU = Electric Propulsion Unit
ERE = Electric Reaction Engine
GSO = Geostationary Orbit
GTO = Geo-transition Orbit
GD = Gyrodine, single-gimbal control gyro
IRF = Inertial Reference Frame
GMC = Gyroscopic Moment Cluster
MRP = Modified Rodrigues Parameters
ORF = Orbital Reference Frame
PWM = Pulse-width Modulation
RM = Rotational Maneuver
SC = Spacecraft

1 Introduction

The first attempts to create low-orbit satellite communication systems failed in the early 2000s mainly due to economic factors. Currently, this idea is being persistently imposed in connection with the increased challenges on the globality, speed and volume of information exchange. Various countries have started implementing such systems, consisting of thousands of minisatellites in low orbits. A decent response of the space communications technology [Testoyedov et al., 2017] based on geostationary platforms, stands up to these challenges. Such platforms are assembled in geostationary orbit (GSO) by space robot-manipulators from replaceable and replenished components, and then regularly serviced by the SRMs for several decades.

Modern achievements in research and development of space robots are presented in review articles [Moosavian and Papadopoulos, 2007; Flores-Abad et al., 2014; Li et al., 2019; Papadopoulos et al., 2021]. We study a SRM with an initial mass of 6300 kg which was launched to an initial elliptical geo-transition orbit (GTO) with perigee r_π=6571 km (altitude of 200 km), apogee r_α=42164 km (altitude of 35793 km) and the inclination i=51.6 deg. The spacecraft (SC) attitude and orbit control system (AOCS) has the following drives: a chemical propulsion unit (CPU) with the thrust P^{c}=200 N, a plasma electric propulsion unit (EPU) with thrust P^{e}=0.58 N, an EPU based on 8 catalytic electric reaction engines (EREs) with pulse-width modulation (PWM) of their thrust, and a gyroscopic moment cluster (GMC) based on 4 single-gimbal control moment gyroscopes – gyrodines (GDs).

Measurement of the kinematic parameters of the SRM spatial motion is carried out by a strapdown inertial navigation system with correction by signals of the GPS/GLONASS satellites and star trackers. If the distance becomes less than 500 m, these parameters relative to a geostationary satellite (*target*) are also determined using the video cameras and lidars.

The strategy used for the SRM launching on the GSO according to a combined scheme contains two stages:

(i) moving the SRM to the GTO with perigee r_π = 17571 km (altitude of 11,000 km) using the CPU;

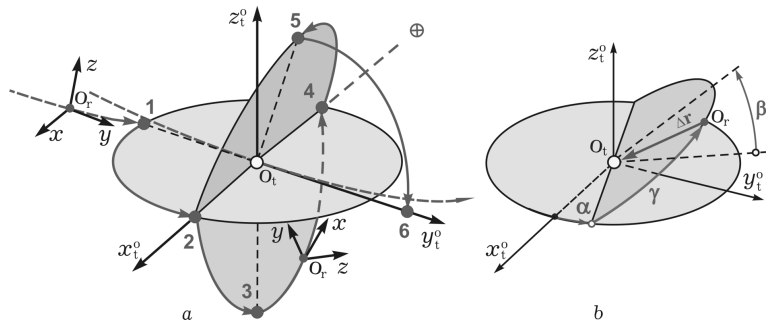

Figure 1. The SRM flyby scheme during visual inspection of a geostationary satellite state

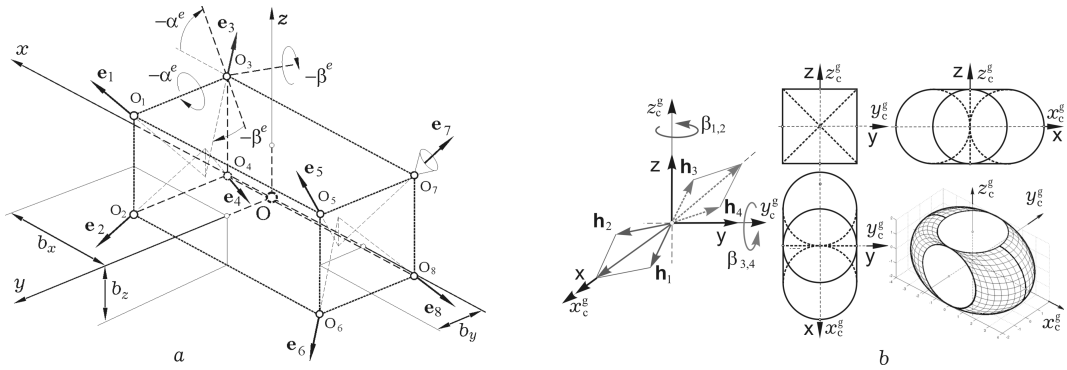

Figure 2. The schemes of EPU with 8 catalytic EREs (a) and GMC based on 4 gyrodines (b)

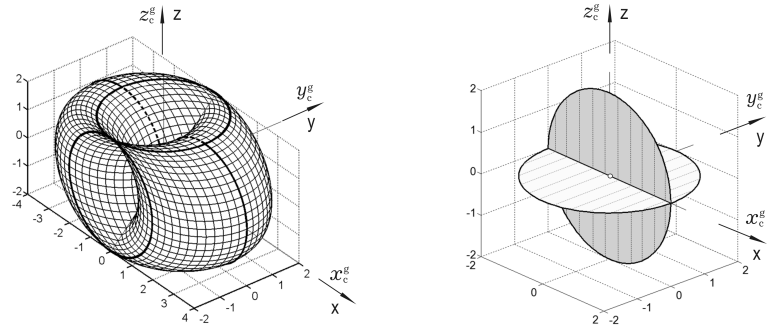

Figure 3. Main sets of natural singular states for the GMC's scheme *2-SPE* in canonical reference frame

(ii) additional launching (*add-launching*) of the SRM from achieved elliptical GTO to GSO with radius $r_g = 42164$ km (altitude of 35786 km) using the plasma EPU and GMC by multi-step transition to an orbit close to the GSO with an accuracy of 58 km [Somov et al., 2020a; Somov et al., 2020b; Somov et al., 2021c].

For motions of the SRM and target on GSO it is very difficult to solve the above key problems. Here, it is necessary to take into consideration the forward and rotational motion of both the target and controlled SRM according to the laws of the space flight mechanics in the gravitational fields of the Earth, Moon and Sun, and also taking into account the influence of solar pressure forces, namely within the theory of photogravitational celestial mechanics [Polyakhova, 2011] with careful consideration of the fundamental physics for spacecraft motion.

This paper deals with two problems: (i) synthesis of the guidance and control laws for the SRM when it is approaching a target to the distance of 50 m and next a visual inspecting of its technical state, Fig. 1; (ii) a dynamical analysis of the spacecraft both forward and attitude [Somov et al., 2021b] motions during these modes.

2 Models and the Problem Statement

To perform the considered modes, the AOCS uses the plasma and catalytic EPUs as well as the GMC based on GDs with own angular momentum (AM) $\mathrm{h}_g = 30$ Nms.

We apply the inertial reference frame (IRF), notation $\{\cdot\} = \mathrm{col}(\cdot)$, $[\cdot] = \mathrm{line}(\cdot)$, $(\cdot)^{\mathrm{t}}$, $[\cdot\times]$ and $\circ$, $\tilde{}$ for vectors, matrices and quaternions, as well as $[\alpha]_i$ for the matrix of elementary rotation about i-th axis by an angle α, $i = 1,2,3 \equiv 1 \div 3$. The orbital reference frames (ORFs) of the SRM $\mathrm{O_r}x^{\mathrm{o}}y^{\mathrm{o}}z^{\mathrm{o}}$ with a pole $\mathrm{O_r}$ and the target $\mathrm{O_t}x_{\mathrm{t}}^{\mathrm{o}}y_{\mathrm{t}}^{\mathrm{o}}z_{\mathrm{t}}^{\mathrm{o}}$ with a pole $\mathrm{O_t}$ are used, as well as the SRM body reference frame (BRF) $\mathrm{O_r}xyz$.

We assume that the SRM is equipped with a telescope with an axis of sight parallel to the BRF $\mathrm{O_r}y$ axis (Fig. 1a). The location of the target in the robot's BRF is determined by the vector $\Delta\mathbf{r}(t)$, see Fig. 1b.

The thrust vector $\mathbf{P}^{\rm c}$ of the CPU is directed along the axis $\mathrm{O}_r y$, as is the thrust vector $\mathbf{P}^{\rm e}$ of a plasma EPU. In EPU scheme with 8 catalytic EREs (Fig. 2*a*) we present the unit vectors $\mathbf{e}_p$, $p=1\div 8$ of the ERE nozzle axes.

Assume that the vector $\boldsymbol{\rho}_p$ defines the point O_p at which the thrust vector of the p-th ERE is applied. Each catalytic ERE has the PWM of its thrust $p_p(t)$, which is described by the nonlinear continuous-discrete relation

$$p_p(t)=\mathrm{P}^{\rm m}\,\mathrm{PWM}(t-T^{\rm e}_{zu},t_r,\tau_m,\mathrm{v}_{p\,r})\;\forall t\in[t_r,t_{r+1}),$$

$t_{r+1}=t_r+T^{\rm e}_u$, $r\in\mathbb{N}_0\equiv[0,1,2,\dots)$ with period $T^{\rm e}_u$ and a time delay $T^{\rm e}_{zu}$. Here $\mathrm{P}^{\rm m}$ is the nominal value of a thrust, similar for all catalytic EREs, and the function

$$\mathrm{PWM}(t,t_r,\tau_m,\mathrm{v}_{pr})\equiv\begin{cases}\mathrm{sign}\,\mathrm{v}_{pr} & t\in[t_r,t_r+\tau_{pr}),\\ 0 & t\in[t_r+\tau_{pr},t_{r+1});\end{cases}$$

$$\tau_{p\,r}\equiv\begin{cases}0 & |\mathrm{v}_{p\,r}|\le\tau_m,\\ \mathrm{sat}\,(T^{\rm e}_u,\ |\mathrm{v}_{p\,r}|) & |\mathrm{v}_{p\,r}|>\tau_m.\end{cases}$$

In the BRF, the thrust vector of p-th ERE is calculated as $\mathbf{p}_p(t)\equiv\{\mathrm{p}_p\}=-p_p(t)\,\mathbf{e}_p$, and vectors of the EPU thrust $\mathbf{P}^e\equiv\mathbf{P}=\{\mathrm{P}_i\}$ and torque $\mathbf{M}^{\rm e}$ are computed by formulas $\mathbf{P}^e(t)=\Sigma\,\mathbf{p}_p(t)$ and $\mathbf{M}^{\rm e}(t)=\Sigma\,[\boldsymbol{\rho}_p\times]\mathbf{p}_p(t)$.

Column $\boldsymbol{\mathcal{H}}(\boldsymbol{\beta})=\mathrm{h}_g\Sigma\mathbf{h}_p(\beta_p)=\mathrm{h}_g\mathbf{h}(\boldsymbol{\beta})$ presents the AM vector for the GMC by scheme *2-Scissored Pair Ensemble* (*2-SPE*) [Crenshaw, 1973] based on 4 GDs, see Fig. 2*b* where $|\mathbf{h}_p|=1$, $p=1\div4$, and h_g is a constant own AM of each GD. The vector $\mathbf{M}^{\rm g}=\{\mathrm{M}^{\rm g}_i\}$ of the GMC control torque is represented by the relations

$$\mathbf{M}^{\rm g}=-\boldsymbol{\mathcal{H}}'=-\mathrm{h}_g\mathbf{A}_{\rm h}(\boldsymbol{\beta})\,\mathbf{u}^{\rm g}_k(t);\ \dot{\boldsymbol{\beta}}=\mathbf{u}^{\rm g}_k(t)\equiv\{\mathrm{u}^{\rm g}_{pk}(t)\}$$

$\forall k\in\mathbb{N}_0\equiv[0,1,2,\dots)$ with a period T_u of digital control $\mathrm{u}^{\rm g}_{pk}(t)=\mathrm{Zh}[\mathrm{sat}(\mathrm{qntr}(u^g_{pk},u^{\rm o}_g),u^{\rm m}_g),T_u]$, a vector column $\boldsymbol{\beta}=\{\beta_p\}$, a matrix $\mathbf{A}_{\rm h}(\boldsymbol{\beta})=\partial\mathbf{h}(\boldsymbol{\beta})/\partial\boldsymbol{\beta}$ and symbol $(\cdot)'$ of local time derivative.

The *2-SPE* scheme singular state is appeared when *Gram* matrix $\mathbf{G}(\boldsymbol{\beta})=\mathbf{A}_{\rm h}(\boldsymbol{\beta})\mathbf{A}^{\rm t}_{\rm h}(\boldsymbol{\beta})$ loses its full rang, i.e. when $\mathsf{G}(\boldsymbol{\beta})\equiv\det\mathbf{G}(\boldsymbol{\beta})=0$. Figure 3 show main sets of natural singular states for this GMC's scheme in canonical reference frame $\mathrm{O}x^{\rm g}_{\rm c}y^{\rm g}_{\rm c}z^{\rm g}_{\rm c}$ [Somov, 2016].

In IRF, the robot's orientation is determined by quaternion $\boldsymbol{\Lambda}=(\lambda_0,\boldsymbol{\lambda})$, $\boldsymbol{\lambda}=\{\lambda_i\}$, $i=1\div3$. We use a vector of modified Rodrigues parameters (MRP) $\boldsymbol{\sigma}=\mathbf{e}\tan(\Phi/4)$ with Euler unit vector $\mathbf{e}$ and angle Φ of own turn which is uniquely connected with quaternion $\boldsymbol{\Lambda}$ by explicit relations. Kinematic equations for vector $\mathbf{r}_r$ of the robot's location and quaternion $\boldsymbol{\Lambda}$ have the form $\mathbf{r}'_{\rm r}+\boldsymbol{\omega}\times\mathbf{r}_{\rm r}=\mathbf{v}_r$ and $\dot{\boldsymbol{\Lambda}}=\boldsymbol{\Lambda}\circ\boldsymbol{\omega}/2$, and dynamics of its spatial motion is represented as follows

$$\begin{gathered}m\,(\mathbf{v}'_r+\boldsymbol{\omega}\times\mathbf{v}_r)=\mathbf{P}^{\rm e}+\mathbf{F}^{\rm d};\\ \dot{\mathbf{K}}+\boldsymbol{\omega}\times\mathbf{G}=\mathbf{M}^{\rm g}+\mathbf{M}^{\rm e}+\mathbf{M}^{\rm d}.\end{gathered}\qquad(1)$$

Here $\mathbf{v}_r$ (index r, *robot*) is the velocity vector of SRM forward motion; vector $\mathbf{G}=\mathbf{K}+\boldsymbol{\mathcal{H}}(\boldsymbol{\beta})$, where $\mathbf{K}=\mathbf{J}\boldsymbol{\omega}$ is vector of the SRM angular momentum, and the $\mathbf{F}^{\rm d}$ and $\mathbf{M}^{\rm d}$ are the vectors of external disturbing forces and torques. The vectors $\mathbf{r}_t$ and $\mathbf{v}_t$ (index t, *target*) represent the geostationary satellite's location and velocity of its forward motion. The vectors of range to the target $\Delta\mathbf{r}=\{\Delta\mathrm{r}_i\}$ and difference $\Delta\mathbf{v}=\{\Delta\mathrm{v}_i\}$ between the velocities of the SRM and the target are calculated by ratios $\Delta\mathbf{r}=\mathbf{r}_t-\mathbf{r}_r$ and $\Delta\mathbf{v}=\mathbf{v}_t-\mathbf{v}_r$.

Estimates of the CPU fuel consumption (of 3,100 kg) and duration (of 7 days) of the SRM interorbital flight to GTO with perigee altitude of 11,000 km were obtained [Somov et al., 2020a] by known methods. As a result, the 3200 kg SRM is then add-launching to the GSO using a plasma electric propulsion.

The SRM should be placed not just to "ideal" GSO, but to the vicinity of the nominal standing of the communications satellite in its specific predicted orbit, close to the GSO. If we assume that the SRM add-launch to the target standing point is completed with an accuracy of 57.7 km, the duration of add-launch is 92.62 days with 123 orbit revolutions and fuel consumption of 197.32 kg [Somov et al., 2021c]. As a result, the 3000 kg SRM is beginning approach to the target using a plasma EPU.

We study the problems of approaching to target and visual checking its technical state by the SRM as a solid (1), controlled by both the plasma EPU and GMC with reversals of the SRM body as well as its spatial stabilization using the EPU based on eight catalytic EREs with PWM of their thrust.

3 The Guidance and Control Laws

Let us assume that at initial time moment $t_{\rm i}$, the vectors of the location and velocity of the forward motion are known in the IRF for the SRM $\mathbf{r}_r(t_{\rm i})$, $\mathbf{v}_r(t_{\rm i})$ and target $\mathbf{r}_t(t_{\rm i})$, $\mathbf{v}_t(t_{\rm i})$. Here it is convenient to apply a cylindrical reference frame [Elyasberg, 1965] when coordinates are the values of radial r and angle u of its deviation from an arbitrary direction in the reference plane, as well as the lateral offset z in the direction orthogonal to this plane. The SRM forward motion is determined by relations $\mathbf{r}_r=\{rC_u,rS_u,z\}$; $\mathbf{v}_r=\{\dot rC_u-rS_u\dot u,\dot rS_u+rC_u\dot u,\dot z\}$, where $S_u\equiv\sin u$ and $C_u\equiv\cos u$.

Assume that w^r,w^t and w^z are the radial, transversal, and lateral components of the SRM control acceleration vector, and μ is the gravitational parameter of the Earth. The SRM approach to a target in central gravitational field over a time $t\in[t_{\rm i},t_{\rm f}]$ is described by equations

$$\ddot r-r\dot u^2+\mu/r^2=w^r;\ r\ddot u+2\dot r\dot u=w^t;\ \ddot z+\mu\,z/r^3=w^z$$

under boundary conditions

$$\begin{gathered}\mathrm{v}^r(t_{\rm i})=\langle\mathbf{v}_r(t_{\rm i}),\mathbf{e}^r_{\rm i}\rangle,\ \mathrm{v}^r(t_{\rm f})=\langle\mathbf{v}_t(t_{\rm f}),\mathbf{e}^r_{\rm f}\rangle;\\ \mathrm{v}^t(t_{\rm i})=\langle\mathbf{v}_r(t_{\rm i}),\mathbf{e}^t_{\rm i}\rangle,\ \mathrm{v}^t(t_{\rm f})=\langle\mathbf{v}_t(t_{\rm f}),\mathbf{e}^t_{\rm f}\rangle;\\ \mathrm{v}^z(t_{\rm i})=\langle\mathbf{v}_r(t_{\rm i}),\mathbf{e}^z_{\rm i}\rangle,\ \mathrm{v}^z(t_{\rm f})=\langle\mathbf{v}_t(t_{\rm f}),\mathbf{e}^t_{\rm f}\rangle;\\ u(t_{\rm i})=\varphi_{\rm i},\ u(t_{\rm f})=\varphi_{\rm i}+\arccos(\langle\mathbf{e}^r_{\rm i},\mathbf{e}^r_{\rm f}\rangle),\end{gathered}$$

where the unit vectors $\mathbf{e}$ with different indices are calculated using the following relations:

$$\begin{gathered}\mathbf{e}^r_{\rm i}=\mathbf{r}_r(t_{\rm i})/r_r(t_{\rm i});\ \mathbf{e}^r_{\rm f}=\mathbf{r}_t(t_{\rm f})/r_t(t_{\rm f});\\ \mathbf{e}^{\rm v}_{\rm i}=\mathbf{v}_r(t_{\rm i})/\mathrm{v}_r(t_{\rm i});\ \mathbf{e}^{\rm v}_{\rm f}=\mathbf{v}_t(t_{\rm f})/\mathrm{v}_t(t_{\rm f});\\ \mathbf{e}^z_{\rm i}=\mathbf{e}^r_{\rm i}\times\mathbf{e}^{\rm v}_{\rm i},\mathbf{e}^z_{\rm f}=\mathbf{e}^r_{\rm f}\times\mathbf{e}^{\rm v}_{\rm f};\ \mathbf{e}^t_{\rm i}=\mathbf{e}^z_{\rm i}\times\mathbf{e}^r_{\rm i},\mathbf{e}^t_{\rm f}=\mathbf{e}^z_{\rm f}\times\mathbf{e}^r_{\rm f}.\end{gathered}$$

Here, a forecast of target's location $\mathbf{r}^p_t(t)$ and velocity $\mathbf{v}^p_t(t)$ vectors is made on a time interval $t\in[t_{\rm i},t_{\rm f}]$ and

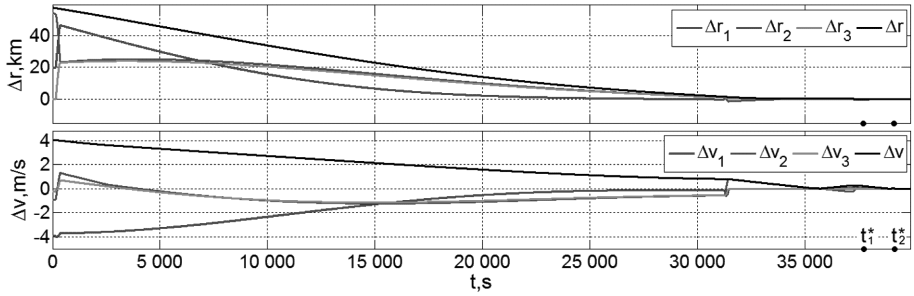

Figure 4. The differences in the position and velocity vectors of the target and space robot

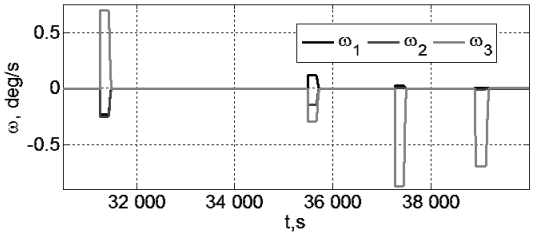

Figure 5. The angular velocity vector of the SRM at its RMs

vectors $\mathbf{r}_t(t_\mathrm{f})$, $\mathbf{v}_t(t_\mathrm{f})$ are calculated by the known analytical relations [Elyasberg, 1965; Battin, 1999].

The law of the SRM positional guidance is determined by the vectors $\mathbf{r}_r^p(t)$, $\mathbf{v}_r^p(t)$ and acceleration $\mathbf{w}_r^p(t)$. Dynamical processes of the SRM approaching to target and its visual inspecting are described by the difference $\Delta\mathbf{r}(t)=\mathbf{r}_t(t)-\mathbf{r}_r(t)$ between vectors of the target and SRM positions as well as the difference $\Delta\mathbf{v}(t) = \mathbf{v}_t(t)-\mathbf{v}_r(t)$ between the vectors of their velocities.

When synthesizing the SRM guidance law for its long-term flight with small electric propulsion, it is necessary to carefully take into account the influence of the gravitational fields of the Earth, Moon and Sun as well as solar pressure forces.

Here, we for the first time apply a forecasting the influence of these perturbations. Such a forecast should be performed in the SRM onboard computer, its results are used in the synthesis of the guidance law, which provides small errors when the specified boundary conditions are met at the end of the SRM flight, first for a range of 500 m and then at a range of 50 m.

The simplest discrete algorithms for switching on/off the plasma EPU are applied at the time moments, which are formed onboard the SRM according to the laws of its positional guidance.

Discrete control algorithm of the catalytic EPU uses a vector $\delta\Delta\mathbf{r}_r = \Delta\mathbf{r}_r^p - \Delta\mathbf{r}_r$ of mismatch between the program difference $\Delta\mathbf{r}_r^p \equiv \Delta\mathbf{r}^p(t_r)$ and the measured difference $\Delta\mathbf{r}_r \equiv \Delta\mathbf{r}(t_r)$; the values $\delta\Delta\mathbf{r}_r$ are formed in the robot's BRF with a period T_u^e at the time moments t_r. In this algorithm, using the recurrent relations

$$\mathbf{g}_{r+1}^\mathrm{e}=k_b^\mathrm{e}\mathbf{g}_r^\mathrm{e}-k_c^\mathrm{e}\delta\Delta\mathbf{r}_r;\,\tilde{\mathbf{p}}_r=k_u^\mathrm{e}(\mathbf{g}_r^\mathrm{e}-k_p^\mathrm{e}\delta\Delta\mathbf{r}_r)$$

at first the vector $\mathbf{P}_r^{ep}$ of the catalytic EPU thrust *pulse* over semi-interval $t\in[t_r,t_{r+1})$ is calculated in the form

$$\mathbf{P}_r^{ep}=m\,T_u^\mathrm{e}(\mathbf{C}_r^\mathrm{e}\mathbf{w}_r^p+\tilde{\mathbf{p}}_r),$$

and then the durations $\tau_{p\,r}$ of the PWM thrust activation for all eight EREs are computed by explicit formulas [Somov et al., 2017].

For the SC attitude guidance law $\mathbf{\Lambda}^p(t)$, $\boldsymbol{\omega}^p(t)$, $\boldsymbol{\varepsilon}^p(t)$ the error quaternion $\mathbf{E}=(e_0,\mathbf{e})=\tilde{\mathbf{\Lambda}}^p\circ\mathbf{\Lambda}$ with $\mathbf{e}=\{e_i\}$, corresponds to the error matrix $\mathbf{C}^\mathrm{e}=\mathbf{I}_3-2[\mathbf{e}\times]\mathbf{Q}_\mathrm{e}^\mathrm{t}$ with $\mathbf{Q}_\mathrm{e}=\mathbf{I}_3e_0+[\mathbf{e}\times]$, and to the MRP vector $\boldsymbol{\sigma}^\mathrm{e}=\mathbf{e}^\mathrm{e}\,\tan(\Phi^\mathrm{e}/4)$ as well as the angular error vector $\delta\boldsymbol{\phi}=\{\delta\phi_i\}=4\boldsymbol{\sigma}^\mathrm{e}$. The error vector $\delta\boldsymbol{\omega}$ on angular velocity is calculated by the ratio $\delta\boldsymbol{\omega}=\boldsymbol{\omega}-\mathbf{C}^\mathrm{e}\boldsymbol{\omega}^p$.

In algorithm of the SRM attitude control, the vectors of angular mismatch $\boldsymbol{\epsilon}_k=-\delta\boldsymbol{\phi}_k$, angular velocity $\boldsymbol{\omega}_k$ and $\mathbf{G}_k=\mathbf{J}\boldsymbol{\omega}_k+\boldsymbol{\mathcal{H}}_k$ are determined to calculate the required control torque vector $\mathbf{M}_k^\mathrm{g}$ of the GMC as follows

$$\mathbf{g}_{k+1}^\mathrm{g}=k_b^\mathrm{g}\,\mathbf{g}_k^\mathrm{g}+k_c^\mathrm{g}\,\boldsymbol{\epsilon}_k;\;\tilde{\mathbf{m}}_k=k_u^\mathrm{g}(\mathbf{g}_k^\mathrm{g}+k_p^\mathrm{g}\boldsymbol{\epsilon}_k);$$
$$\mathbf{M}_k^\mathrm{g}=\boldsymbol{\omega}_k\times\mathbf{G}_k+\mathbf{J}(\mathbf{C}_k^\mathrm{e}\boldsymbol{\varepsilon}_k^p+[\mathbf{C}_k^\mathrm{e}\boldsymbol{\omega}_k^p\times]\boldsymbol{\omega}_k+\tilde{\mathbf{m}}_k),$$

and then vector $\mathbf{M}_k^\mathrm{g}$ is distributed between the GDs by explicit relations [Matrosov and Somov, 2004; Somov, 2016]. As a result, the GMC digital control vector $\mathbf{u}_k^\mathrm{g}(t)=\mathbf{u}_k^\mathrm{g}$ is formed $\forall\,t\in[t_k,t_{k+1})$.

4 The SRM Approach to Geostationary Satellite

The flight of the SRM with a mass $m=3000$ kg and the inertia tensor $\mathbf{J}=\mathrm{diag}(3248,\,2348,\,3640)$ kg m^2 was studied when approaching the target at the standing point of 76 deg East GSO from a range of 57.7 km to a distance of 50 m. With these data, the synthesis of the SRM guidance law was carried out with minimizing the fuel consumption of a plasma EPU when its four inclusions of thrust $\mathrm{P}^\mathrm{e}=0.58$ N. A dynamic analysis of the

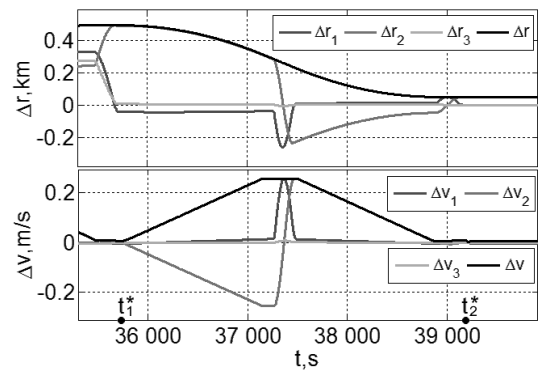

Figure 6. The differences at the 2-nd part of the approaching

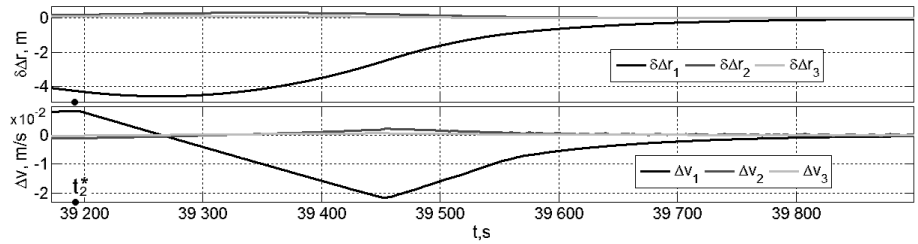

Figure 7. Mismatches in the position and differences in the velocity at the stage of the SRM spatial stabilization

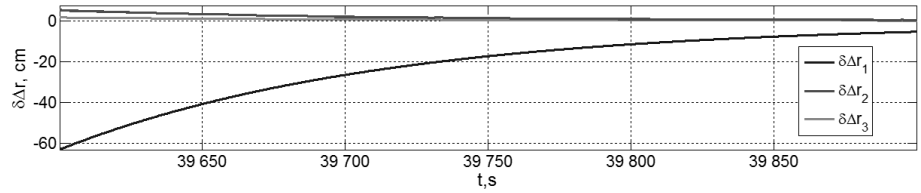

Figure 8. Mismatches in the SRM position at the end of its spatial stabilization

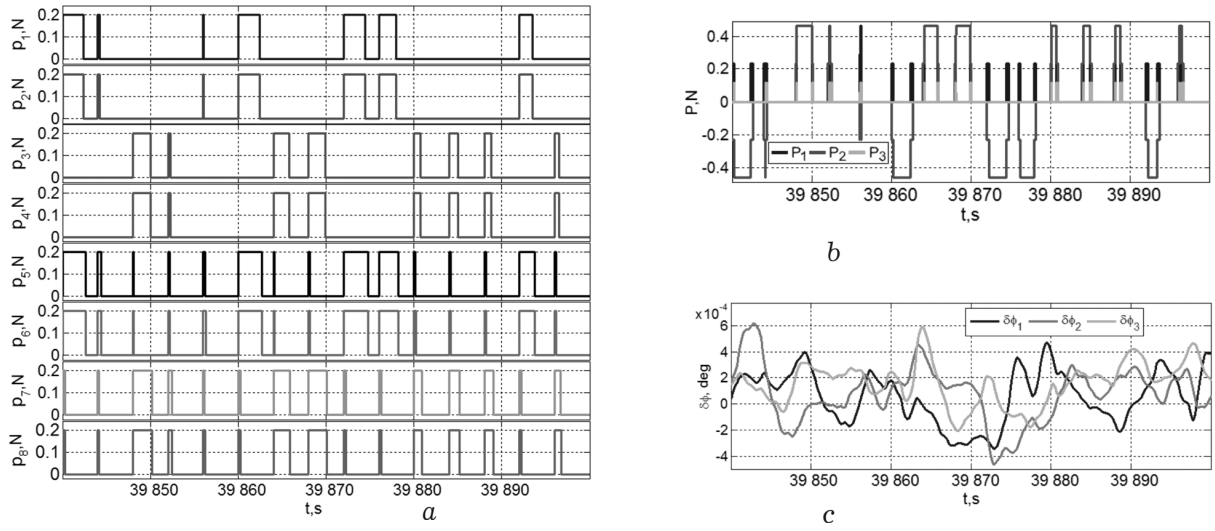

Figure 9. The PWM thrusts of catalytic EREs, the EPU thrusts and the SRM angular errors at the end of its stabilization

SRM approach was performed for the model (1) with the attitude digital control law when its period $T_u = 0.5$ s and the gyrodyne's AM value $\mathrm{h}_g = 30$ Nms.

Figure 4 presents changes in the vectors of target location and velocity difference when the SRM is approaching a range of 50 m at the time interval $t \in [0, 39900]$ s. Here, a time t is counted from the conditional value $t_0 = 0$ when the robot's BRF matches its ORF, the coordinates are highlighted in color, namely blue on yaw axis x, green on roll axis y and red on pitch axis z, and the modules of vectors are marked in black. The following approach stages are performed, see Figs. 4 – 9:

• at 1-st part of SRM approach on a range of 500 m:
(1i) the 1-st rotational maneuver (RM-1) of the SRM $\forall t \in [154, 394)$ s by an angle of 53.72 deg;
(1ii) the acceleration pulse of a plasma EPU thrust $\forall t \in [394, 2585)$ s at the SRM fixed orientation;
(1iii) free flight of SRM $\forall t \in [2585, 31257)$ s and regular pointing of solar array panels at the Sun;
(1iv) the RM-2 of the SRM $\forall t \in [31257, 31497)$ s by an angle of 133.60 deg, see Fig. 5;
(1v) the brake pulse of a plasma EPU thrust $\forall t \in [31497, 35482)$ s at the SRM constant orientation;
(1vi) the RM-3 of the robot $\forall t \in [35482, 35722)$ s by an angle of 65.02 deg.

This part of SRM approach is ended in the time mo-

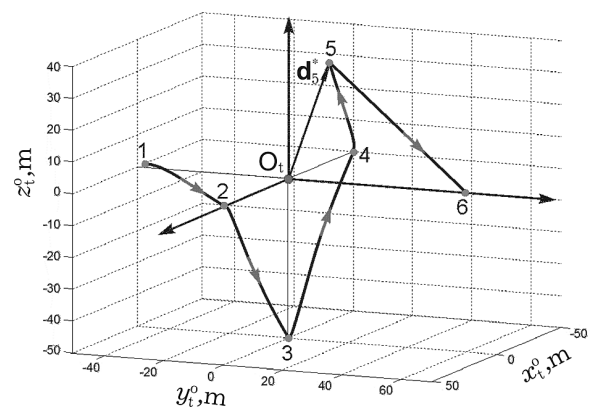

Figure 10. The SRM flybys scheme with a plasma EPU

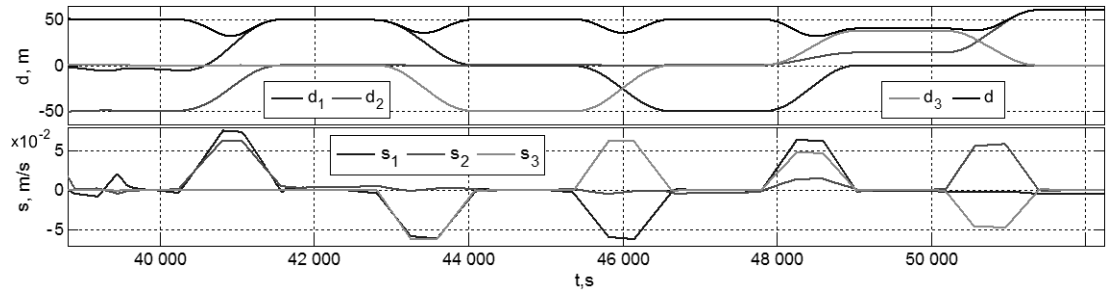

Figure 11. Changing the vectors of the SRM distance and velocity relative the target in its orbital reference frame

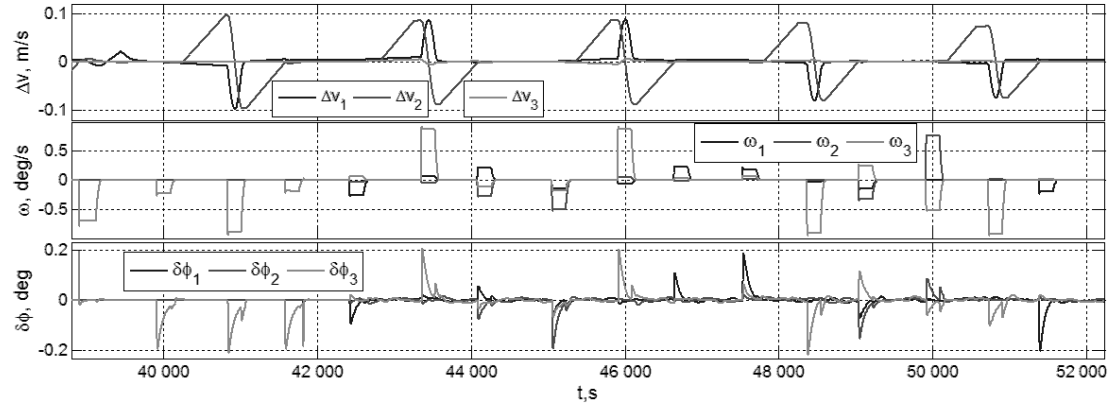

Figure 12. Changing the vectors of difference between velocities, the SRM angular velocity and angular error in its body reference frame

ment $t = t_1^\star = 35722$ s with the accuracy $\Delta \mathrm{r} = 50.97$ m and $\Delta \mathrm{v} = 0.03$ m/s in the implementation of the specified boundary conditions;

• at 2-nd part of SRM approach on a range of 50 m:
(2i) free flight and angular stabilization of the SRM $\forall t \in [35722, 35743)$ s and its preparing to approach the target at a distance of 50 m, see Fig. 6 ;
(2ii) the acceleration pulse of the EPU thrust $\forall t \in [35743, 37160)$ s at the SRM fixed orientation;
(2iii) free flight $\forall t \in [37160, 37504)$ s and RM-4 $\forall t \in [37264, 37504)$ s by an angle of 173.43 deg;
(2iv) the brake pulse of the plasma EPU thrust $\forall t \in [31497, 35482)$ s at the SRM constant orientation;
(2v) RM-5 $\forall t \in [35482, 35722)$ s by angle 101.67 deg.

This part of SRM approach is ended at the time moment $t = t_2^\star = 39192$ s. Total fuel consumption of the plasma EPU is 302 grams, with its four inclusions at this approach during 10.89 hours.

Subsequent spatial stabilization of the SRM relative to the target for a time $t \geq t_2^\star$ and a given range vector $\Delta \mathbf{r}^p(t) \equiv \mathbf{d}$ with the module $d = |\mathbf{d}| = 50$ m is performed using EPU with the PWM of thrust 8 catalytic EREs when $\mathrm{P^m} = 0.2$ N, $T_u^{\mathrm{e}} = 4$ s, and also the GMC with the period $T_u = 0.5$ s of digital control. The changes of a position mismatch vector $\delta \Delta \mathbf{r}(t) = \mathbf{d} - \Delta \mathbf{r}(t)$ and a velocity difference vector $\Delta \mathbf{v}(t) = \mathbf{v}_t(t) - \mathbf{v}_r(t)$ of the target and SRM at the stage of its spatial stabilization are presented in Fig. 7, and mismatches in the SRM position at the end of its stabilization – in Fig. 8.

Figures $9a$ and $9b$ show the pulse-width modulated thrusts of 8 catalytic EREs and the thrust vector of the catalytic EPU, respectively, at the end of the SRM stabilization mode, and Fig. $9c$ – the SRM angular errors at the same time interval. In this mode for the time interval $t \in [39192, 39900]$ s, the fuel consumption of the catalytic EPU is 83 grams.

5 The SRM Guidance and Control at a Checking

In the ORF of the target, it is convenient to set the SRM movements between the points of the target's inspection observation with a plane $\mathbf{P}$, the position of which is assigned by fixed angles α and β in Fig. $1b$, and with the position of the SRM pole $\mathrm{O_r}$ in this plane, which is determined by the angle $\gamma(t)$ and modulus $d(t) = \Delta r(t)$ (*distance*) of vector $\mathbf{d}(t) \equiv -\Delta \mathbf{r}(t)$, see Fig. $1b$, and also vector $\mathbf{s}(t) \equiv -\Delta \mathbf{v}(t)$ (*speed*).

Previously, we studied spatial guidance SRM as a program location vector $\mathbf{d}(t)$ of the SRM pole $\mathrm{O_r}$ in the plane $\mathbf{P}$ and a program orientation of the axis $\mathrm{O_r}y$ along the vector $\Delta \mathbf{r}$ when the axis $\mathrm{O_r}z$ of the robot's BRF is directed along the normal to the plane of its movement [Somov et al., 2021a], see Fig. $1a$.

In this mode, the SRM's spatial movement is implemented by the catalytic EPU and GMC. The disadvantage of this approach is the high fuel consumption of the catalytic EPU.

Let's assume that during the visual inspecting the target's state six points with numbers $n = 1 \div 6$ correspond to vectors $\mathbf{d}_n^*$ of the SRM's mass center positions which are determined in the target's ORF $\mathrm{O_t}x_{\mathrm{t}}^{\mathrm{o}} y_{\mathrm{t}}^{\mathrm{o}} z_{\mathrm{t}}^{\mathrm{o}}$ using the

orthogonal matrices $\mathbf{Q}_n = [\alpha_n]_3^{\mathrm{t}} [\beta_n]_1^{\mathrm{t}} [\gamma_n]_3^{\mathrm{t}}$ and their modules $d_n^* = |\mathbf{d}_n^*|$, namely
$d_1^* = d_2^* = d_3^* = d_4^* = 50$ m, $d_5^* = 40$ m and $d_6^* = 60$ m.
Here we have proposed and investigated a different approach: all SRM's inspection flybys between the observing points are performed using a plasma EPU (Fig. 10), and catalytic EPU is applied only to stabilize the SRM position. For this mode the simulation results are presented in Figs. 11 and 12.

6 Conclusion

Some problems on guidance and control of a space robot-manipulator when its approaching a geostationary satellite by electric thrust for visual inspecting the satellite technical state were studied.

Using the developed algorithms of the robot's attitude and orbit control system the simulation results were presented that demonstrate the algorithms effectiveness.

The main achievement of this paper is a minimizing of fuel consumption of the electric propulsion units when visual inspecting of a geostationary satellite state.

Acknowledgements

The work was supported by Russian Foundation for Basic Research, Grant no. 20-08-00779.

References

Battin, R. (1999). *An Introduction to the Mathematics and Methods of Astrodynamics*. AIAA, Reston.

Crenshaw, J. (1973). 2-SPEED, a single-gimbal moment gyro attitude control system. *AIAA Paper*, (73-895), pp. 1–10.

Elyasberg, P. (1965). *Introduction to the Theory of Flight of Artificial Earth Satellites*. Nauka, Moscow.

Flores-Abad, A., Ma, O., Pham, K., and Ulrich, S. (2014). A review of space robotics technologies for on-orbit servicing. *Prog. Aerosp. Sci.*, **68**, pp. 1–26.

Li, W., Cheng, D., Liu, X., and et all. (2019). On-orbit service (OOS) of spacecraft: A review of engineering developments. *Prog. Aerosp. Sci.*, **108** (2), pp. 32–120.

Matrosov, V. and Somov, Y. (2004). Nonlinear problems of spacecraft fault tolerant control systems. In *Nonlinear Problems in Aviation and Aerospace*, vol. 12, pp. 309–331. CRC Press / Taylor & Francis.

Moosavian, S. and Papadopoulos, E. (2007). Free-flying robots in space: an overview of dynamics modeling, planning and control. *Robotica*, **25** (5), pp. 537–547.

Papadopoulos, E., Aghili, F., Ma, O., and Lampariello, R. (2021). Robotic manipulation and capture in space: A survey. *Front. Robot. AI*, **8** (686723), pp. 1–36.

Polyakhova, E. (2011). *Space Flight with a Solar Sail: Problems and Prospects*. Librocom, Moscow.

Somov, Y. (2016). Guidance, navigation and control of information satellites: Methods for modeling, synthesis and nonlinear analysis. *Math. Eng. Sci. Aerosp.*, **7** (2), pp. 223–248.

Somov, Y., Butyrin, S., and Somov, S. (2021a). Autonomous attitude and orbit control of a space robot inspecting a geostationary satellite. *J. Phys. Conf. Ser.*, **1864** (012132), pp. 1–7.

Somov, Y., Butyrin, S., and Somov, S. (2021b). Dynamics of an autonomous spacecraft control system at initial transition to a tracking mode. *Cybern. Phys.*, **10** (3), pp. 185–190.

Somov, Y., Butyrin, S., Somov, S., and Somova, T. (2020a). Launching a space robot in orbit and approaching to geostationary satellite. *Izvestiya of Samara Scientific Centre RAS*, **22** (2), pp. 124–131. In Russian.

Somov, Y., Butyrin, S., Somov, S., and Somova, T. (2020b). Nonlinear digital and pulse-width control at approaching a space robot with a geostationary satellite. *Math. Eng. Sci. Aerosp.*, **11** (4), pp. 993–1001.

Somov, Y., Butyrin, S., and Somova, T. (2021c). Guidance and control of a space robot at additional launching and approaching a communication geostationary satellite. In *2021 8th IEEE Intern. Workshop on Meteorology for AeroSpace*, Naples, pp. 572–577.

Somov, Y., Starinova, O., and Butyrin, S. (2017). Pulse-width control of electro-reaction engines for a station-keeping of a land-survey satellite on sun-synchronous orbit. *Procedia Eng.*, **185**, pp. 267–274.

Testoyedov, N., Rayevsky, V., Somov, Y., Titov, G., and Yakimov, Y. (2017). Attitude and orbit control systems of Russian communication, navigation and geodesic satellites: History, present and future. *IFAC-PapersOnLine*, **50** (1), pp. 6422–6427.